Chemical Engineering Journal Advances 12 (2022) 100401

Contents lists available at ScienceDirect

Chemical Engineering Journal Advances

journal homepage: www.sciencedirect.com/journal/chemical-engineering-journal-advances

Comparison between graphene-water and graphene oxide-water nanofluid flows over exponential shrinking sheet in porous medium: Dual solutions and stability analysis

Ajeet Kumar Verma [a], Sohita Rajput [a], Krishnendu Bhattacharyya [a,*], Ali J. Chamkha [b], Dhananjay Yadav [c]

[a] Department of Mathematics, Institute of Science, Banaras Hindu University, Varanasi, Uttar Pradesh 221005, India
[b] Faculty of Engineering, Kuwait College of Science and Technology, Doha District, Kuwait
[c] Department of Mathematical and Physical Sciences, University of Nizwa, Oman

ARTICLE INFO

Keywords:
Nanofluid
Graphene/graphene oxide nanoparticles
Exponential shrinking sheet
Porous medium
Dual solutions
Stability analysis

ABSTRACT

To achieve ultra-high cooling rate requirement of modern-day industries the combined use of nanofluid and porous medium in several engineering and industrial processes provides excellent outcomes. In present analysis, the comparison between the flows of Gr-w and GO-w nanofluids over exponential shrinking sheet inside porous medium is investigated. Governing coupled PDEs are changed into ODEs by appropriate transformations which are solved numerically with the help of shooting method with RK4; and obtained dual solutions of Darcy flow for certain enforced mass suction exist and consequently, a stability analysis is performed to test physical stability of both solutions which proves physical stability of upper solution branch and instability of lower solution branch. The impacts of several physical parameters are presented in graphical modes along with a tabular comparison. The study reveals that Gr-w nanofluid delays the boundary layer flow separation more in comparison with GO-w nanofluid and hence, the requirement of mass suction for existence of Gr-w nanofluid flow is of lower amount. Also, consideration of porous material as flow medium defers the separation phenomenon. The rise of surface-drag force is witnessed for porous medium and mass suction and it is relatively larger for Gr-w nanofluid than GO-w nanofluid in case of upper branch solution and the surface cooling rate is larger for Gr-w nanofluid in comparison with GO-w nanofluid.

1. Background of the investigation

The studies on heat transfer in the flow over stretching/shrinking surface are popularised for its real-world utilizations in various fields of engineering and industry, such as glass blowing, paper production, artificial fiber and extraction of polymer, extrusion, etc. [1]. Firstly, Crane [2] gave solution in closed form of viscous boundary layer flow past linear stretched sheet. Erickson et al. [3] and Fox et al. [4] introduced suction/injection in the flow over moving flat plates for uniform temperature and plate velocity. Gupta and Gupta [5] extends Erickson's [3] problem by taking linearly proportional surface velocity instead of constant velocity. For flow over power-law stretched sheet, Ali [6] concluded that suction augments the heat transfer, while blowing has opposite impact. The flow over exponential expanding sheet was elaborated by Magyari and Keller [7]. Elbashbeshy [8] reported that suction provides better cooling over a continuously expanding sheet in exponential form. The influences of viscous dissipation and buoyancy on flow past exponential stretched sheet with exponential variable wall temperature were analyzed by Partha et al. [9]. The flow on shrinking sheet was firstly elaborated by Wang [10]. Miklavčič and Wang [11] and Wang [12] determined that existence of flow over shrinking surfaces is possible if sufficient amount of suction is imposed or if stagnation point flow velocity is assumed and additionally, Miklavčič and Wang [11] gave existence-uniqueness condition for flow over shrinking sheet. After the above conclusion flow over shrinking surfaces in various physical aspects were analyzed by several researchers [13–15]. Bhattacharyya [16] demonstrated that flow over exponential shrinking sheet is possible with certain condition on mass suction and found more than one solution. Bhattacharyya and Pop [17] described that flow past exponential shrinking sheet exists with lesser amount of suction due to introduction of magnetic field. Whereas Bhattacharyya and Vajravelu [18] illustrated

* Corresponding author.
E-mail addresses: sohita.math@gmail.com (S. Rajput), krish.math@yahoo.com (K. Bhattacharyya).

https://doi.org/10.1016/j.ceja.2022.100401

Available online 13 September 2022

Nomenclature

a	A positive constant (ms^{-1})
C_f	Skin-friction coefficient
c_p	Specific heat at constant pressure ($Jkg^{-1}K^{-1}$)
F^*	Perturbation function
$f(\eta)$	Dimensionless stream function
$f'(\eta)$	Dimensionless velocity
G	Perturbation function
Gr-w	Graphene-water
GO-w	Graphene oxide-water
k	Variable permeability (m^2)
k_0	A non-negative constant (m^2)
K	Permeability parameter
L	Reference length (m)
Nu_x	Local Nusselt number
Pr	Prandtl number
q_w	Wall heat flux (Wm^2)
Re_x	Local Reynolds number
S	Wall mass transfer parameter
T	Temperature (K)
T_0	Reference temperature (K)
T_w	Temperature at sheet (K)
T_∞	Ambient temperature (K)
t	Time (s)
u, v	Velocity components along x- and y-axes (ms^{-1})
U_w	Variable shrinking velocity (ms^{-1})
v_w	Suction/injection velocity (ms^{-1})
v_0	A constant (ms^{-1})
x, y	Cartesian coordinates measured along and normal to the sheet, respectively (m)

Greek symbols

ρ	Density (kgm^{-3})
μ	Dynamic viscosity ($kgm^{-1}s^{-1}$)
υ	Kinematic viscosity (m^2s^{-1})
ϕ	Nanoparticle volume fraction
ϕ_1,ϕ_2	Nanoparticle volume fraction related parameters
η	Similarity variable
ψ	Stream function
ξ	Time dependent variable
γ^*	Growth/decay rate of the perturbation
γ_1^*	Smallest eigenvalue
κ	Thermal conductivity ($Wm^{-1}K^{-1}$)
τ_w	Wall shear stress ($kgm^{-1}s^{-2}$)
ρc_p	Effective heat capacity ($JK^{-1}m^{-3}$)
$\theta(\eta)$	Dimensionless temperature

Subscript

nf	Nanofluid
f	Base fluid
s	Solid particle

that similarity solution existence range of velocity-ratio parameter is higher for stagnation-point flow on shrinking sheet when velocity of contraction is considered exponentially.

The flows in solid matrix with pores, which are linked and occupied with fluid so that fluid motion exists through these pores, are familiar as porous medium flow. Utilizing porous materials in thermal systems enhances flow mixing significantly due to chaotic movements of fluids through relevant pores and also it expands heat transfer area dramatically, which improves heat exchange rate significantly. Hence, porous medium received noticeable attention of the researcher in recent years for the utilization in the field of heat transfer. Porous medium is utilized in the field of heat exchanger, oil production, ground water flow, etc. The flow through porous medium was proposed by Darcy in 1856. The Darcy's experimental flow model characterizes a simple linear relationship between the flow rate and drop of pressure inside porous media. Chauhan and Agarwal [19] provides numerical and an approximate solution of MHD flow inside porous medium over expanding sheet and demonstrated that flow velocity augmented with permeability parameter. Vyas and Srivastava [20] concluded that temperature augments, whereas temperature gradient decline with permeability parameter when flow taking place over expanding sheet inside porous medium. Later, Rosali et al. [21] revealed shrinking sheet flow in porous medium and they explored enlargement of solution range for solution existence with less permeability of porous medium. Vyas and Srivastava [22] explored radiative heat transfer in boundary layer flow over exponential shrinking sheet inside porous medium and concluded that lesser suction required for existence of solution in presence of porous medium. Later, Jain and Choudhary [23] described MHD slip flow on exponential shrinking sheet in porous material and they obtained the temperature enhancement/decrement for first/second solution of the acquired dual solutions with permeability of Darcy porous material. Recently, Animasaun [24] and Motsa and Animasaun [25] considered non-Darcian flow in their investigation.

A strong need of ultrahigh cooling performance in industry and engineering is not yet achieved with conventional coolants (like ethylene glycol, water, oil, etc.) due to their poor thermal properties. Also, the suspensions containing millimetre or micrometre sized particles are not suitable for heat transfer due to rapid settling clogging and augment in pressure drop [26]. So, a new type of fluid introduced by Choi [27] which is able to overcome above shortcomings in achieving ultrahigh cooling are classified as nanofluids. Nanofluids are engineered by stable and uniform suspension of particles with nanometre sized (1–100 nm), called nanoparticles in liquids. From number of experiments, it is clear that very low concentration of nanoparticles shown distinctive feature of thermal performance, such as augmentations of thermal conductivities [28,29]. Also, thermal conductivity is nonlinearly related with concentration [30,31]. Due to the above key role and various industrial utilizations, such as electronics, transportation, thermal therapy for cancer treatment, nanodrug delivery, chemical processes, and cooling processes of nanofluid [32], it is grabbing serious attention of modern-day researchers. The flow of nanofluids was governed by existing two models given by Buongiorno [33] and Tiwari and Das [34]. Khan and Pop [35] firstly incorporated impacts of Brownian motion and thermophoresis towards flow on expanding sheet. Ishak et al. [36] deduced that skin friction, Nusselt and Sherwood number rise with stretching effect. Dero et al. [37] demonstrated the augmentations of cooling rate with Brownian motion, thermophoresis and Eckert number in analysis of Casson nanofluid flow on expanding/contracting sheet. The second law of thermodynamics for MHD nanofluid over porous shrinking surface was analyzed by Rashid et al. [38]. Recently, Reddy et al. [39]; Rawat and Kumar [40], Yang et al. [41], Khan and Nadeem [42], Jumana et al. [43] and Tshivhi and Makinde [44] considered several aspects of nanofluid flow for expanding/shrinking sheet. Naramgari and Sulochana [45] demonstrated enquiry of heat-mass transfer in nanofluid flow on exponentially expanding sheet inside porous material. Li et al. [46] analyzed Williamson nanofluid over exponential stretching surface. Ali et al. [47] deduced that velocity of the flow field augments with stretching ratio. Nanofluid flow over exponential stretching/shrinking sheet was done by Zainal et al. [48,49]. Ghosh and Mukhopadhyay [50] in their investigation of nanofluid flow on exponentially shrinking sheet established that temperature rises with Brownian motion, while it declines with volume fraction of nanoparticle. Later, the researchers, Ghosh and

Mukhopadhyay [51], Shi et al. [52] and Waini et al. [53] described several aspects of nanofluid flow past shrinking surface which shrinks exponentially. Some recent studies on nanofluid over various surfaces exploring various key properties may be revealed in relevant literature [54–62].

The heat transfer efficiency of nanofluids further escalates when the flow medium is a porous medium and this concurrent occurrence is quite useful in several thermal systems. The enhanced thermal properties of nanofluids are further improved since contact surface area between solid and fluid becomes large when they pass through porous medium [63]. Hayat et al. [64] explained MHD nanofluid flow over expanding sheet inside porous medium. Nayak et al. [65] obtained the decline of flow velocity for resistive force of the porous matrix inside nanofluid flow on exponential expanding sheet. Sharma et al. [66] examined the attributes of 3-D MHD nanofluid flow past contracting sheet inside porous media in presence of thermal radiation and heat generation and reported that flow velocity and temperature diminished with permeability parameter. The heat transfer characteristics of nanofluid in presence of thermal radiation and porous medium over contracting sheet was done by Haq et al. [67] and authors have obtained dual solutions for velocity and temperature; it was found that temperature of the flow decline with porous medium parameter for both the solution branches. Shawky et al. [68] assessed numerically the 2-D Williamson nanofluid flow in a porous media over expanding sheet and found that Nusselt number augmented with porosity parameter. Lately, Tadesse et al. [69,70] and Dey et al. [71] explored several usable properties of nanofluid flow in porous medium.

Graphene (Gr) has honeycomb like structure and having monomolecular layer of carbon atoms, while when graphene oxidized with O functional groups forms two-dimensional material are familiar as graphene oxide (GO). Firstly, sir second Baronent Benjamin Colline Brodie in 1859 synthesized GO via oxidation of nitric acid and potassium chloride with bulk graphite. Presently, GO is synthesized with modified hummers method. The industrial and engineering utilizations of Gr are in electronics, medical sciences, sensing outlets, and energy sector [72], while that of GO are in computer storage system, turbine system, turbo machinery hard disk, jet motors and centrifugal pump rotating blades [73]. Graphene nanoparticles have high thermal conductivity, expanded surface area, fast mobility of electrons, and stability [74]. Upadhya et al. [75] concluded that graphene-water dusty nanofluid have superior heat transfer characteristics than Ag-Water dusty nanofluid in their study on stretched cylinder. Sharma et al. [76] conferred unsteady flow of graphene nanofluid and reported the decline of velocity with porosity. Hussain et al. [77] illustrated the flow over expanding sheet in porous medium and demonstrated the high cooling with thermal radiation, thermal slip and unsteadiness. Aly [78] obtained multiple solutions over expanding/ shrinking sheet for Gr-water(Gr-w) nanofluid. Rashid et al. [79] described the remarkable role of spherical shape of Gr-nanoparticles in comparison with lamina shape for high heat transfer rate in Marangoni flow of Gr-water nanofluid. The thermal conductivity enhancement of Jeffery nanofluid for graphene nanoparticles was enlightened by Sandeep and Malvandi [80]. Gul et al. [81] demonstrated a comparative analysis of Marangoni convection of water and ethylene glycol having graphene oxide nanoparticles and explored that GO-ethylene glycol nanofluid have better cooling efficiency than that of GO-water(GO-w) nanofluid. Hamid et al. [82] discussed the stability of flow of magnetic graphene oxide nanofluid. Heat transfer in water-based GO nanofluid asymmetric channel flow was explained by Javanmard et al. [83] and they showed that GO-nanoparticles escalate heat transfer within the channel.

The above literature demonstrates that boundary layer flow over exponential shrinking sheet separate from the sheet, this motivates us to consider the influence of porous medium to investigate either it delays the separation or accelerates it. The different molecular structures of Gr and GO with interesting thermal properties act as another piece of motivation towards the investigation of both types of nanofluids (Gr-w and GO-w) on an exponential shrinking sheet in a porous material. Overhead literature survey also reveals that there is no study which concerns the porous medium impact over exponential shrinking sheet and comparative influences of Gr-w and GO-w nanofluids with variable mass suction. Therefore, the problem is completely novel and not yet recognized. Influences of all the flow governing parameters on velocity, temperature fields and materials of engineering importance, i.e., local skin-friction and local Nusselt number have been shown graphically and illustrated. This problem has several applications in electronics, medical field, paper production, and extrusion of plastic films. In this investigation the scientific answers to the following research questions are tried to be addressed:

(i) The requirement of mass suction for the existence of steady-state boundary layer flow for Gr-w and GO-w nanofluid flow over exponential shrinking sheet in presence of porous medium.
(ii) The comparative analysis of thermal performance of Gr-w and GO-w nanofluids and their impacts on velocity, temperature, surface-drag and cooling rate on the shrinking sheet flow in presence of porous medium and mass suction.
(iii) The requirement of mass suction for the existence of steady-state boundary layer flow over shrinking sheet for various values of permeability parameter in presence of nanoparticles.
(iv) The influences of porous medium resistance on velocity, temperature, surface-drag and cooling rate in presence of nanoparticles.

2. Formulation and fundamental equations

Consider steady 2D nanofluid boundary layer flow with graphene/graphene oxide nanoparticles on an exponential shrinking sheet in porous regime. The considered surface is supposed to be porous and through which a variable wall mass suction/injection is imposed. A physical drawing of this problem is specified in Fig. 1. The fundamental equations for motion and energy distribution may be taken as [64]:

$$\frac{\partial u}{\partial x}+\frac{\partial v}{\partial y}=0 \tag{1}$$

$$u\frac{\partial u}{\partial x}+v\frac{\partial u}{\partial y}=\upsilon_{nf}\frac{\partial^2 u}{\partial y^2}-\frac{\upsilon_{nf}}{k}u \tag{2}$$

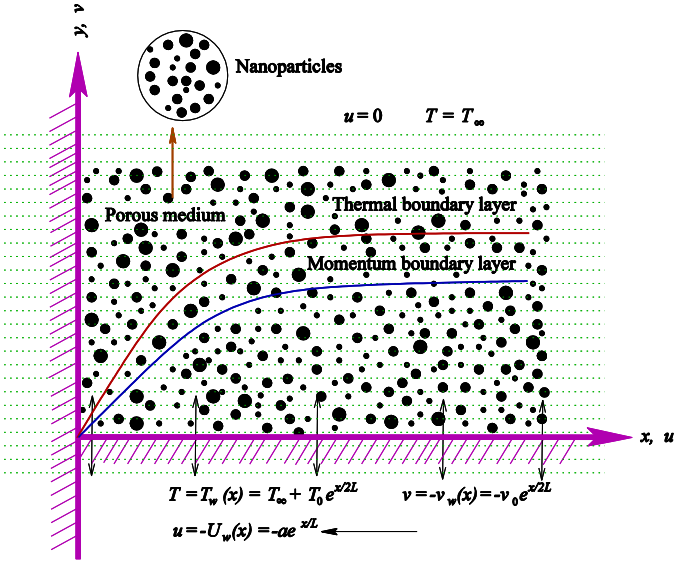

Fig 1. Physical sketch of the flow.

$$u\frac{\partial T}{\partial x}+v\frac{\partial T}{\partial y}=\frac{\kappa_{nf}}{(\rho c_p)_{nf}}\frac{\partial^2 T}{\partial y^2} \tag{3}$$

subject to [16]

$$\left.\begin{aligned} u=-U_w,\ v=-v_w(x),\ T=T_w(x)=T_\infty+T_0e^{x/2L}\ \text{at}\ y=0,\\ u\to 0,\ T\to T_\infty,\ \text{as}\ y\to\infty, \end{aligned}\right\} \tag{4}$$

where u and v denotes respectively velocity components along x- and y-directions, $k=k_0/e^{\frac{x}{L}}$ gives variable permeability of porous medium with k_0 being a non-negative constant, T represents temperature of nanofluid, $U_w=ae^{x/L}$ is variable shrinking velocity with a being positive constant having dimension LT^{-1}, $v_w=v_0e^{x/2L}$ is variable velocity of suction/injection with $v_0(>0/<0)$ being a constant, T_0 and L denote reference temperature and length, υ_{nf} is kinematic viscosity of nanofluid, $(\rho c_p)_{nf}$ is heat capacity of nanofluid, κ_{nf} represents thermal conductivity of nanofluid, which are defined as [84]:

$$\begin{aligned} \upsilon_{nf}&=\frac{\mu_{nf}}{\rho_{nf}},\\ \rho_{nf}&=(1-\phi)\rho_f+\phi\rho_s,\\ \mu_{nf}&=\frac{\mu_f}{(1-\phi)^{2.5}},\\ (\rho c_p)_{nf}&=(1-\phi)(\rho c_p)_f+\phi(\rho c_p)_s,\\ \kappa_{nf}&=\frac{(\kappa_s+2\kappa_f)-2\phi(\kappa_f-\kappa_s)}{(\kappa_s+2\kappa_f)+\phi(\kappa_f-\kappa_s)}\kappa_f. \end{aligned}$$

Here, μ_{nf} and ρ_{nf} are viscosity and density of nanofluid, respectively, μ_f, ρ_f, $(\rho c_p)_f$ and κ_f are viscosity, density, specific heat capacity and thermal conductivity of base fluid, respectively, ρ_s, $(\rho c_p)_s$ and κ_s are density, specific heat capacity and thermal conductivity of solid nanoparticles, respectively, ϕ represents solid volume fraction of nanoparticles. Here two types of nanoparticles, namely, graphene and graphene oxide, with spherical shape and water as base fluid are considered and their thermal properties are given in Table 1.

The continuity Eq. (1) is satisfied with introduction of stream function ψ so that

$$u=\frac{\partial\psi}{\partial y}\ \text{and}\ v=-\frac{\partial\psi}{\partial x}.$$

Also, introducing following self-similar transformations [53]:

$$\left.\begin{aligned} u=ae^{x/L}f'(\eta),\ v=-\sqrt{\frac{a\upsilon_f}{2L}}e^{x/2L}[f(\eta)+\eta f'(\eta)],\\ \eta=\sqrt{\frac{a}{2L\upsilon_f}}e^{x/2L}y,\ \theta(\eta)=\frac{T-T_\infty}{T_w-T_\infty}. \end{aligned}\right\} \tag{5}$$

Using Eq. (5), from Eqs. (2) and (3) the following self-similar nonlinear equations are finally achieved:

$$\frac{1}{\phi_1}(f'''-Kf')+ff''-2f'^2=0 \tag{6}$$

$$\frac{1}{\phi_2}\frac{\kappa_{nf}}{\kappa_f}\theta''+\Pr(f\theta'-f'\theta)=0 \tag{7}$$

where $K=\frac{2L\upsilon_f}{ak_0}$ is permeability parameter, and $\Pr=\frac{\upsilon_f(\rho c_p)_f}{\kappa_f}$ is Prandtl number. Here $\phi_1=(1-\phi)^{2.5}\left(1-\phi+\phi\frac{\rho_s}{\rho_f}\right)$, $\phi_2=(1-\phi)+\phi\frac{(\rho c_p)_s}{(\rho c_p)_f}$.

The boundary conditions in Eq. (4) reduce to the following forms:

$$\left.\begin{aligned} f(0)=S,\ f'(0)=-1,\ \theta(0)=1,\\ f'(\infty)=0,\ \theta(\infty)=0. \end{aligned}\right\} \tag{8}$$

Here $S=v_0\sqrt{2L/(a\upsilon_f)}$ is wall mass transfer parameter, $S>0$ ($v_0>0$) gives mass suction and $S<0$ ($v_0<0$) gives mass injection.

Quantities of physical importance must be local skin-friction coefficient and local Nusselt number, which are declared as:

$$\begin{aligned} C_f&=\frac{\mu_{nf}}{\rho_f U_w^2}\left(\frac{\partial u}{\partial y}\right)_{y=0}\ \text{and}\\ Nu_x&=-\frac{x\kappa_{nf}}{\kappa_f(T_w-T_\infty)}\left(\frac{\partial T}{\partial y}\right)_{y=0}. \end{aligned} \tag{9}$$

Using Eq. (5) in Eq. (9) we get

$$\begin{aligned} C_f\mathrm{Re}_x^{1/2}&=\frac{1}{(1-\phi)^{2.5}}f''(0)\ \text{and}\\ Nu_x\mathrm{Re}_x^{-1/2}&=-\frac{\kappa_{nf}}{\kappa_f}\theta'(0), \end{aligned} \tag{10}$$

where $\mathrm{Re}_x=2LU_w/\upsilon_f$ is local Reynolds number.

3. Numerical method

Nonlinear differential Eqs. (6) and (7) with (8) form a BVP(boundary value problem) and the solutions are obtained by shooting method [85–87] after changing the BVP into an IVP(initial value problem). During the process, it is required to pick an appropriate finite value of $\eta(\to\infty)$, say η_∞. Also, the following 1st-order system is set:

$$f'=p,\ p'=q,\ q'=\phi_1(2p^2-fq)+Kp, \tag{11}$$

$$\theta'=r,\ r'=\frac{\phi_2\Pr\{\theta p-fr\}}{(\kappa_{nf}/\kappa_f)}, \tag{12}$$

with

$$f(0)=S,\ p(0)=-1,\ \theta(0)=1. \tag{13}$$

To solve Eqs. (11) and (12) with (13) as IVP, values of $q(0)$ and $r(0)$, i.e., $f''(0)$ and $\theta'(0)$ are necessary, but no such values are specified. Initial guesses for $f''(0)$ and $\theta'(0)$ are selected and the 4th order R-K method is applied to achieve the solutions. Later, the computed values of $f'(\eta)$ and $\theta(\eta)$ at $\eta_\infty(=10)$ is compared with stated conditions $f'(\eta_\infty)=0$ and $\theta(\eta_\infty)=0$, and values of initial guesses $f''(0)$ and $\theta'(0)$ are modified by "Secant method" to provide improved approximation of solutions. The step-length is considered as $\Delta\eta=0.01$. The whole procedure is repeated until the solutions are asymptotically convergent with desired accuracy of 10^{-7} level.

4. Stability of the flow

In certain flow conditions, multiple solutions of this problem are obtained and there is a consequent need to know the physical stability of those solutions. Hence, following Merkin [88], the unsteady form of the Eqs. (2) and (3) are considered to examine stability of obtained dual solutions of Eqs. (6) and (7) with (8) and those are specified as:

$$\frac{\partial u}{\partial t}+u\frac{\partial u}{\partial x}+v\frac{\partial u}{\partial y}=\upsilon_{nf}\frac{\partial^2 u}{\partial y^2}-\frac{\upsilon_{nf}}{k}u, \tag{14}$$

$$\frac{\partial T}{\partial t}+u\frac{\partial T}{\partial x}+v\frac{\partial T}{\partial y}=\frac{\kappa_{nf}}{(\rho c_p)_{nf}}\frac{\partial^2 T}{\partial y^2}, \tag{15}$$

where t indicates time and new transformations are

Table 1
Thermophysical properties of water, graphene and graphene oxide nanoparticles (Aly [78] and Hamid et al. [82]).

Physical properties	Water (H_2O)	Graphene (Gr)	Graphene oxide (GO)
$C_p(J/kgK)$	4179	2100	717
$\rho(kg/m^3)$	997.1	2250	1800
$\kappa(W/mK)$	0.613	2500	5000

$$\left.\begin{aligned} &u = ae^{x/L}F'(\eta,\xi),\ v = -\frac{1}{2L}\sqrt{2\upsilon_f La}e^{x/2L}[F(\eta,\xi)+\eta F'(\eta,\xi)],\\ &\eta = \sqrt{\frac{a}{2L\upsilon_f}}e^{x/2L}y,\ \Theta(\eta,\xi) = \frac{T-T_\infty}{T_w-T_\infty},\ \xi = \frac{a}{2L}te^{x/L}. \end{aligned}\right\} \tag{16}$$

Now using above prescribed transformations given by Eq. (16) in Eqs. (14) and (15), we get

$$\frac{\upsilon_{nf}}{\upsilon_f}(F_{\eta\eta\eta} - KF_\eta) + FF_{\eta\eta} - 2F_\eta^2 + 2\xi\left(F_\xi F_{\eta\eta} - F_\eta F_{\eta\xi}\right) - F_{\eta\xi} = 0, \tag{17}$$

$$\frac{\kappa_{nf}/\kappa_f}{(\rho c_p)_{nf}/(\rho c_p)_f}\Theta_{\eta\eta} + \Pr\left\{F\Theta_\eta - F_\eta\Theta + 2\xi\left(F_\xi\Theta_\eta - \Theta_\xi F_\eta\right) - \Theta_\xi\right\} = 0, \tag{18}$$

subject to the boundary conditions

$$\left.\begin{aligned} &F(0,\xi), = S,\ F_\eta(0,\xi) = -1, \Theta(0,\xi) = 1,\\ &\mathrm{F}_\eta(\eta,\xi)\to 0, \Theta(\eta,\xi)\to 0, \text{as}\eta\to\infty. \end{aligned}\right\} \tag{19}$$

Now, to test the stability of steady-state solutions $f(\eta)$ and $\theta(\eta)$ of the BVP Eqs.(6)–(8), we introduce [89]

$$\left.\begin{aligned} &F(\eta,\xi) = f(\eta) + \mathrm{e}^{-\gamma^*\xi}F^*(\eta,\xi),\\ &\Theta(\eta,\xi) = \theta(\eta) + \mathrm{e}^{-\gamma^*\xi}G(\eta,\xi), \end{aligned}\right\} \tag{20}$$

where γ^* is decay or growth rate of disturbance/perturbation functions $F^*(\eta, \xi)$, and $G(\eta, \xi)$, which are small in comparison with $f(\eta)$ and $\theta(\eta)$. We get linearized problem on introduction of Eq. (20) in the Eqs. (17) and (18) as:

$$\frac{\upsilon_{nf}}{\upsilon_f}\left(F^*_{\eta\eta\eta} - KF^*_\eta\right) + fF^*_{\eta\eta} + F^*f'' - 4f'F^*_\eta + 2\xi\left\{f''\left(F^*_\xi - \gamma^*F^*\right) + f'\left(\gamma^*F^*_\eta - F^*_{\eta\xi}\right)\right\} - F^*_{\eta\xi} + \gamma^*F^*_\eta = 0, \tag{21}$$

$$\frac{\kappa_{nf}/\kappa_f}{(\rho c_p)_{nf}/(\rho c_p)_f}G_{\eta\eta} + \Pr\left(fG_\eta - F^*_\eta\theta - f'G + F^*\theta'\right) + 2\xi\Pr\left\{\theta'\left(F^*_\xi - \gamma^*F^*\right) + f'\left(\gamma^*G - \theta_\xi\right)\right\} - \Pr G_\xi + \Pr\gamma^*G = 0, \tag{22}$$

with boundary conditions

$$\left.\begin{aligned} &F^*(0,\xi) = 0,\ F^*_\eta(0,\xi) = 0, \mathrm{G}(0,\xi) = 0,\\ &F^*_\eta(\eta,\xi)\to 0, \mathrm{G}(\eta,\xi)\to 0, \text{as}\eta\to\infty. \end{aligned}\right\} \tag{23}$$

Now, following Weidman et al. [89], to get initial decay/growth of solutions of Eqs. (21) and (22) with Eq. (23), which signifies the stability of steady-state solutions $f(\eta)$ and $\theta(\eta)$, it is required to put $\xi = 0$. Hence, $F^*(\eta,\xi) = F^*_0(\eta)$, and $G(\eta, \xi) = G_0(\eta)$ with $F^*_0(\eta)$ and $G_0(\eta)$ being the initial disturbances to the solutions $f(\eta)$ and $\theta(\eta)$, respectively. In this respect, from Eqs. (21) and (22), we get

$$\frac{\upsilon_{nf}}{\upsilon_f}\left(F^{*'''}_0 - KF^{*'}_0\right) + fF^{*''}_0 + F^*_0f'' - 4f'F^{*'}_0 + \gamma^*F^{*'}_0 = 0, \tag{24}$$

$$\frac{\kappa_{nf}/\kappa_f}{(\rho c_p)_{nf}/(\rho c_p)_f}G''_0 + \Pr\left(fG'_0 - f'G_0 - F^{*'}_0\theta + F^*_0\theta'\right) + \Pr\gamma^*G_0 = 0, \tag{25}$$

with boundary conditions

$$\left.\begin{aligned} &F^*_0(0) = 0,\ F^{*'}_0(0) = 0, G_0(0) = 0,\\ &F^{*'}_0(\eta)\to 0, G_0(\eta)\to 0, \text{as}\eta\to\infty. \end{aligned}\right\} \tag{26}$$

Now, we may have an infinite set of eigenvalues $\gamma^*_1 < \gamma^*_2 < \gamma^*_3$.... on solving the eigenvalue problem Eqs. (24) and (25) with (26) by modifying boundary condition $F^{*'}_0(\eta)\to 0$ as $\eta\to\infty$ with $F^{*\prime\prime}_0(0) = 0$ (Harris et al. [90]). Also, first we will find steady-state solutions $f(\eta)$ and $\theta(\eta)$ with the help of shooting method as mentioned in section (3) then using those steady-state solutions the linearised eigenvalue problem Eqs. (24)–(26) is solved with the help of a computer programming. The stability of steady-state solutions $f(\eta)$ and $\theta(\eta)$ is confirmed by least eigenvalue γ^*_1. If the least eigenvalue is positive ($\gamma^*_1 > 0$) then an initial decay of perturbation will occur, i.e., solutions will be recognised as stable. Whereas, obtained steady-state solutions will be unstable, i.e., an initial growth of perturbation will appear when least eigenvalue is negative ($\gamma^*_1 < 0$).

5. Results and discussion

The impact of porous medium on boundary layer flow is numerically (shooting method) analyzed for Gr-w/GO-w nanofluids over a sheet which shrinks exponentially. At first to validate the numerical scheme and consequent results, a comparison of computed results by present method is exhibited in Table 2 with results of Ghosh and Mukhopadhyay [51] and Waini et al. [53] for water only ($\phi = 0$, i.e., without any nanoparticles) in absence of porous medium ($K = 0$) with $S = 3$, $\Pr = 0.7$ and those are in very good agreements.

The boundary layer flow over exponential shrinking sheet exists if wall mass transfer parameter obeys $S \geq 2.266684$ when there is no nanoparticles and porous medium, i.e., $\phi = 0$ and $K = 0$[16]. Over linearly shrinking sheet to confine generated vorticity inside boundary layer the required amount of mass suction is less ($S \geq 2$ [11]) in comparison with that for exponential shrinking sheet ($S \geq 2.266684$[16]), i.e., more vorticity generated for exponential shrinking sheet than the linear one. The fixed values of the physical parameters throughout the numerical computation are $\phi = 0.05$, $K = 0.2$, $S = 2.5$, and $\Pr = 2$; otherwise, these are mentioned.

Figs. 2 and 3 are sketched to show the deviations of skin-friction coefficient, $C_f\mathrm{Re}_x^{1/2}$ (related to surface-drag) and Nusselt number, $Nu_x\mathrm{Re}_x^{-1/2}$ (related to cooling rate) with S when ϕ varies. From the figures, it is witnessed that multiple (two) solutions exist with $\phi = 0$, 0.05, 0.1 when the critical values of S, say S_c exceed or equal to 2.105280, 2.165338, 2.235618, respectively for Gr-w nanofluid and for GO-w nanofluid the values of S_c must exceed or equal to 2.105280, 2.184649, 2.272930, respectively. However, no solution exists if $S < S_c$, i.e., boundary layer separation occurs, but the boundary layer flow solutions may exist by delaying the separation for $S = 0$(i.e., when the sheet surface is impermeable) and even for $S < 0$(i.e., in case of injection). Actually, for the above two cases of S($S = 0$ and $S < 0$), boundary layer similarity solutions exist only when the permeability of the porous medium is suitably less, i.e., the value of K is appropriately large. From the above-mentioned values of S_c, it is pretty clear that as nanoparticle volume fraction rises in presence of porous medium the vorticity generation is augmented and that's why boundary layer solution range diminishes. Also, Gr-w has larger solution range than GO-w, i.e., vorticity generation is higher in case of GO-w nanofluid than Gr-w nanofluid. It is also evident that when there is no nanoparticle in water, i.e., for clear fluid in porous medium, then vorticity generation is suppressed. Due to presence of solid nanoparticles, the resistive force in the fluid increases and as a consequence vorticity generation rises. Also, Fig. 2 illustrates that $C_f\mathrm{Re}_x^{1/2}$ diminishes with ϕ when S is small ($S \leq 2.5$), but for higher mass suction it boosts with ϕ for upper branch solution and for lower branch it declines. Also, skin-friction escalates with S for upper branch, but opposite behaviour is witnessed for lower branch. Fig. 3 exhibits that $Nu_x\mathrm{Re}_x^{-1/2}$, i.e., surface cooling rate declines with ϕ, whereas opposite nature is seen with S for both solutions branches.

Figs. 4 and 5 portray $C_f\mathrm{Re}_x^{1/2}$ and $Nu_x\mathrm{Re}_x^{-1/2}$ with S for $K = 0$, 0.2, 0.5. It is witnessed from these figures that dual solutions exist when critical values of S, S_c are greater or equal to 2.34422, 2.165338, 1.874169 for Gr-w nanofluid and S_c should equal or exceed 2.36953, 2.184649, 1.883138 for GO-w nanofluid, respectively when $K = 0$, 0.2, 0.5. No solution exists if $S < S_c$, i.e., in these cases mass suction is not sufficient to confine generated vorticity and hence boundary layer

Table 2
Comparison of $f'(0)$ and $-\theta'(0)$ with available literature for $\phi = 0$, $K = 0$, $S = 3$, and Pr $= 0.7$.

	Ghosh and Mukhopadhyay [51]		Waini et al. [53]		Present study	
	Upper branch	Lower branch	Upper branch	Lower branch	Upper branch	Lower branch
$f'(0)$	2.39082	−0.97223	2.390814	−0.972247	2.39080048	−0.97222620
$-\theta'(0)$	1.77124	0.84832	1.771237	0.848316	1.77064610	0.84953457

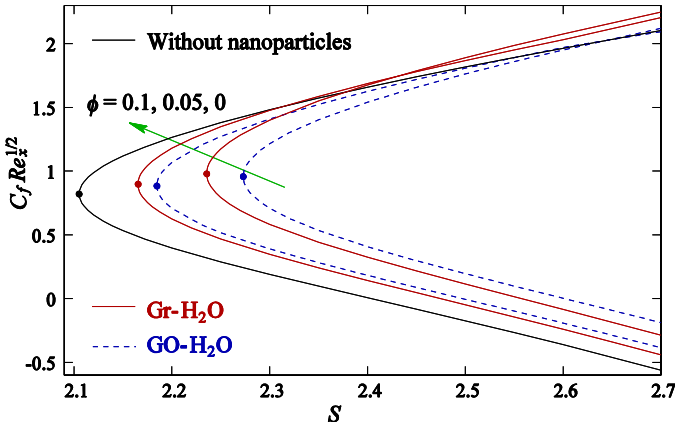

Fig 2. Variation of $C_f \mathrm{Re}_x^{1/2}$ with S for several ϕ.

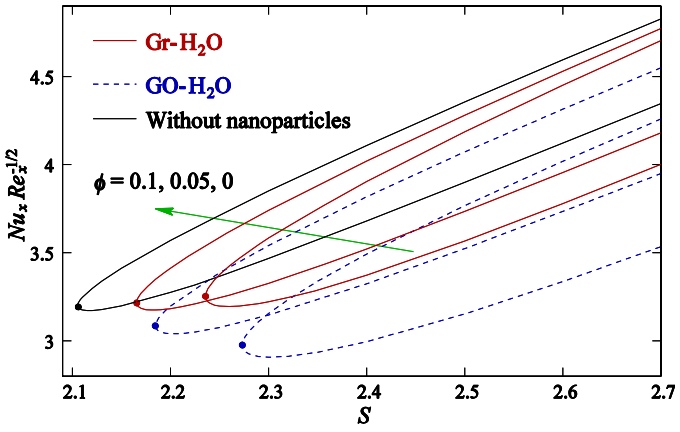

Fig 3. Variation of $Nu_x \mathrm{Re}_x^{-1/2}$ with S for several ϕ.

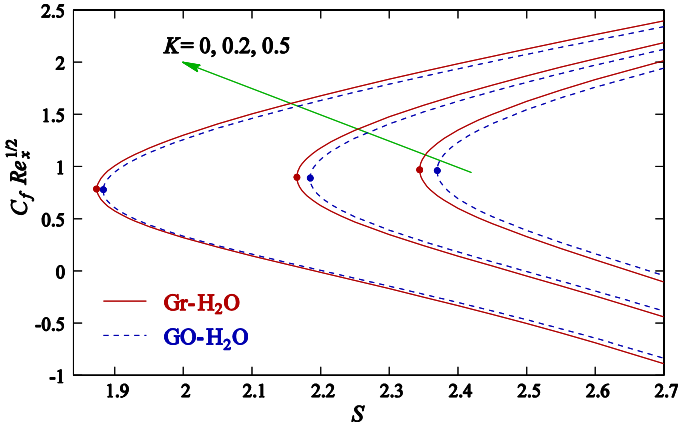

Fig 4. Variation of $C_f \mathrm{Re}_x^{1/2}$ with S for several K.

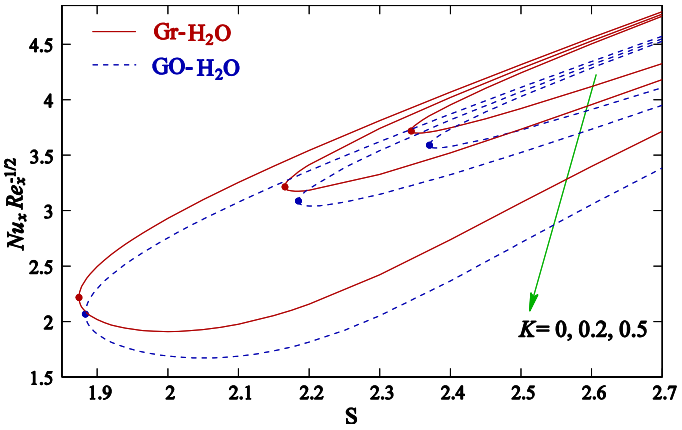

Fig 5. Variation of $Nu_x \mathrm{Re}_x^{-1/2}$ with S for several K.

separation happens. From above critical values of S, it is strongly clear that as K rises the existence range of solution is also augmented, i.e., less amount of mass suction is required for existence of boundary layer flow and solution range of Gr-w nanofluid is greater than GO-w nanofluid, i.e., with higher K the vorticity generation inside boundary diminishes. Physically, augmentation of K results in a low permeable medium and consequently friction and interaction between nanofluids and porous medium boosts, which supresses the vorticity generation due contraction of sheet. From these figures, it is also witnessed that vorticity generation blocks when in presence of nanoparticles permeability parameter K amplifies and solution range of Gr-w nanofluid is higher than GO-w nanofluid. One can points out this as a noteworthy result of the analysis while comparing two nanoparticles: Gr and GO. Fig. 4 conveys that $C_f \mathrm{Re}_x^{1/2}$ escalates with rising K and S for upper branch solution, whereas it weakens for lower branch. Fig. 5 elucidates that $Nu_x \mathrm{Re}_x^{-1/2}$ for upper branch uplifts with K and S, while for lower branch it rises with S and decline with K. Also, from Figs. 2 and 4 we may conclude that surface-drag is comparatively higher for Gr-w nanofluid than GO-w nanofluid.

Fig. 6 predicts the variations $Nu_x \mathrm{Re}_x^{-1/2}$ with S and Pr. This figure elucidates that higher Pr causes growth of the cooling rate coefficient,

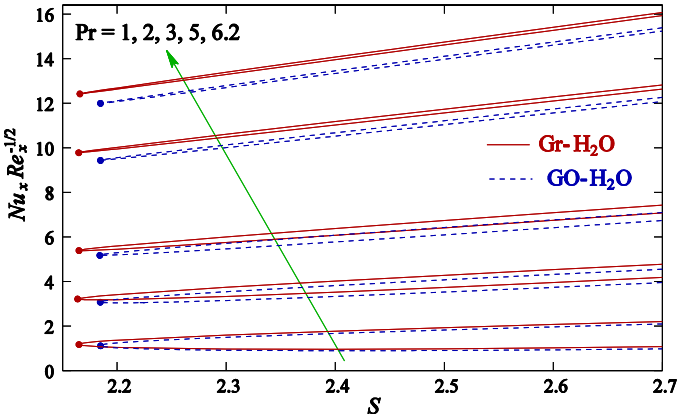

Fig 6. Variation of $Nu_x \mathrm{Re}_x^{-1/2}$ with S for several Pr.

$Nu_x \mathrm{Re}_x^{-1/2}$ for both the solutions, and also $Nu_x \mathrm{Re}_x^{-1/2}$ has lesser values for lower branch than upper branch for a particular Pr. Physically, with rising Pr values thermal diffusivity diminishes. Also, Figs. 3, 5 and 6 demonstrate that cooling rate is higher for Gr-w nanofluid than GO-w nanofluid and this result plays a vital role in choosing appropriate nanoparticle when it is essential.

Figs. 7 and 8 represent the deviations of velocity $f'(\eta)$ and temperature $\theta(\eta)$ for varying ϕ. These figures also confirm the existence of multiple solutions. Fig. 7 portrays that $f'(\eta)$ declines with ϕ for upper branch, whereas it initially diminishes ($\eta < 3$) and later it augments for lower branch. Ultimately, the momentum boundary layer(MBL) widens with ϕ for both the solutions. Fig. 8 depicts that temperature and corresponding thermal boundary layer(TBL) thickness upsurge with ϕ for both solutions. This happens for combine effects of conduction and convection of solid nanoparticles inside the base-fluid. Figs. 9 and 12 elaborate $f'(\eta)$ and $\theta(\eta)$ for several K. Fig. 9 exposes that $f'(\eta)$ amplifies and MBL declines with K for upper branch, whereas $f'(\eta)$ diminishes and MBL augments with K for lower branch. Practically, the resistance in fluid motion escalates in porous medium when K enlarges. Fig. 10 elucidates that $\theta(\eta)$ and corresponding TBL thickness decline for upper branch, however opposite behaviour is observed for lower branch. It is also noticeable that MBL and TBL for lower branch are thicker than upper branch. Figs. 11 and 12 depict $f'(\eta)$ and $\theta(\eta)$ for $S(>0)$. Fig. 11 demonstrates that $f'(\eta)$ elevates and corresponding MBL thickness declines with S for upper branch, whereas opposite character shows in lower branch. Fig. 12 exhibits that $\theta(\eta)$ and TBL thickness suppress with S for both the solutions. Practically, mass suction carries fluid layers to closure of the surface and it results in thinning of boundary layer thickness. This character of mass suction is able to prevent the vorticity diffusion and so, boundary layer separation is deferred. Fig. 13 shows the deviation in $\theta(\eta)$ for varying Pr. It is clear that when Pr augments, $\theta(\eta)$ and corresponding TBL thickness decline for both the solutions. Also, TBL in lower branch is thicker compared to upper branch. Physically, Pr is proportional inversely to thermal conductivity, therefore with smaller Pr nanofluid thermal conductivity grows and hence heat diffusion uplifts. From all the above velocity profiles, it is pretty clear that Gr-w nanofluid have comparatively higher velocity than GO-w nanofluid for upper branch, whereas for lower one the fact is different. Whereas, the temperature for GO-w nanofluid displays higher values than that of Gr-w nanofluid for both solution branches. These results have huge relevance in application view-point.

After the stability analysis for certain values of parameters to confirm the stability of obtained multiple solutions, the upper solution branch is established to be stable and lower solution branch is detected as unstable and in support of the stability claim, the computed values of γ_1^* are provided in Table 3 for few values of S. In this table, for upper solution branches of dual solutions the values of least eigenvalue γ_1^* are positive, whereas γ_1^*'s are negative for lower solution branches.

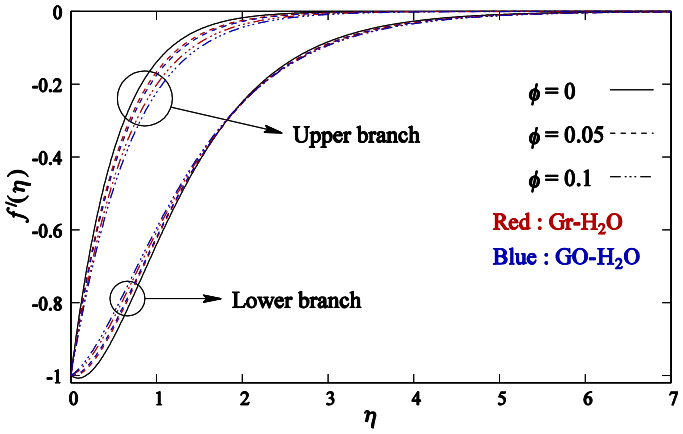

Fig 7. Dual velocity profiles $f'(\eta)$ for several ϕ.

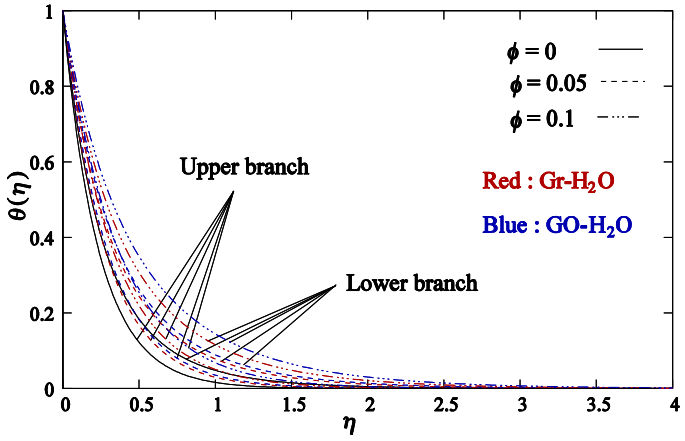

Fig 8. Dual temperature profiles $\theta(\eta)$ for several ϕ.

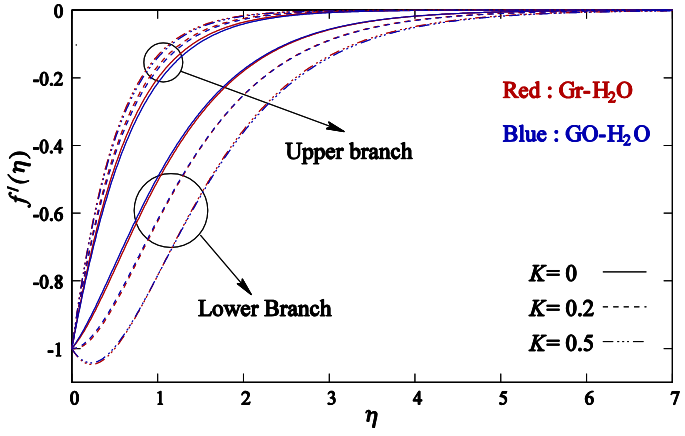

Fig 9. Dual velocity profiles $f'(\eta)$ for several K.

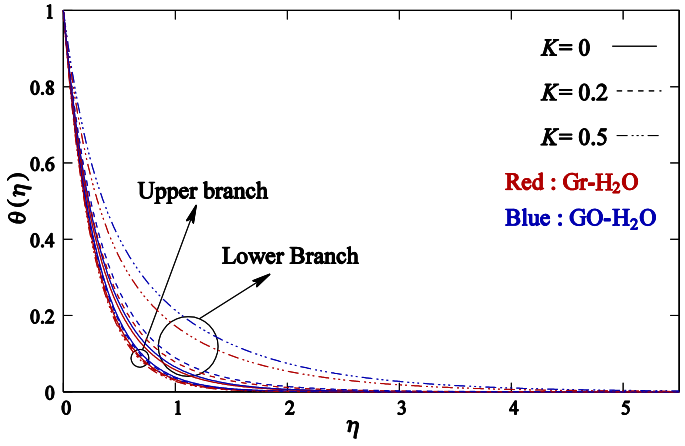

Fig 10. Dual temperature profiles $\theta(\eta)$ for several K.

6. Concluding notes

The steady 2D boundary layer flows of Gr-w nanofluid and GO-w nanofluid over exponential shrinking sheet inside porous medium is numerically analyzed. The main findings of the analysis are given in concise form as:

- The skin-friction for upper branch of Gr-w nanofluids are 1.81707454, 1.86787212 and 1.88916111 when $\phi = 0$, $\phi = 0.05$ and

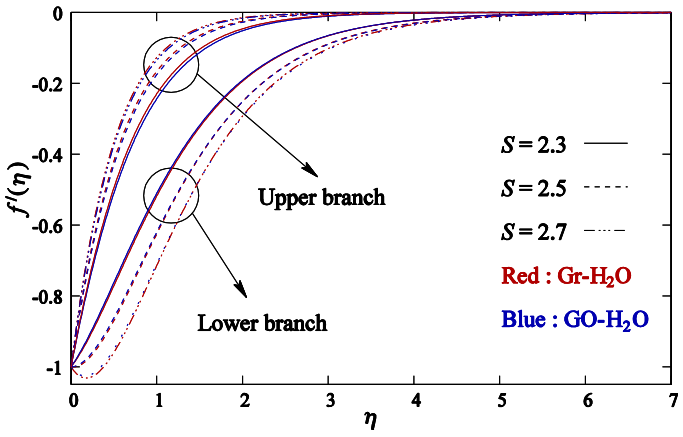

Fig 11. Dual velocity profiles $f'(\eta)$ for several S.

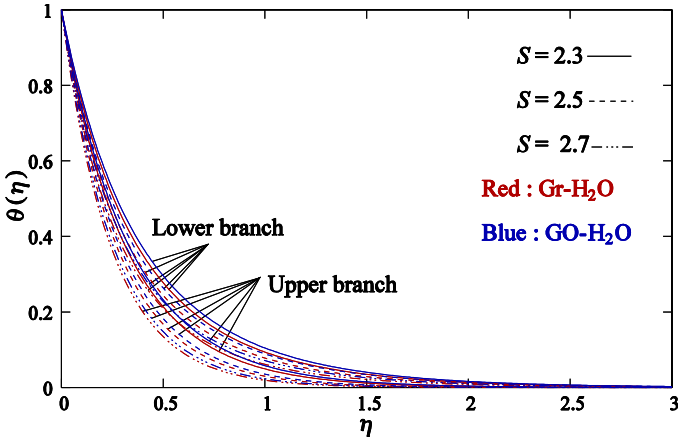

Fig 12. Dual temperature profiles $\theta(\eta)$ for several S.

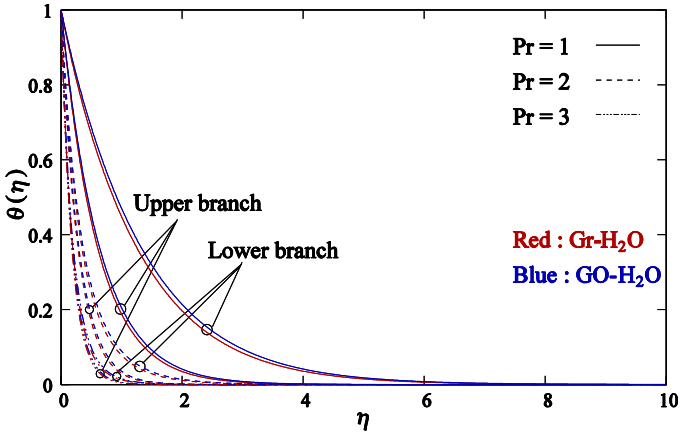

Fig 13. Dual temperature profiles $\theta(\eta)$ for several Pr.

$\phi = 0.1$, respectively and hence it augments by 2.80% when ϕ increases from 0 to 0.05 and it upsurges by 3.97% when ϕ is augmented from 0 to 0.1. While for GO-w nanofluids the values are 1.81707454, 1.80674982 and 1.76219749 when $\phi = 0$, $\phi = 0.05$ and $\phi = 0.1$, respectively; hence it diminishes by 0.57% when ϕ enlarges from 0 to 0.05 and it reduces by 3.02% when ϕ goes from 0 to 0.1.

- The skin-friction for upper branch of Gr-w nanofluids are 1.62420058, 1.86787212 and 2.12571239 when $K = 0$, $K = 0.2$ and $K = 0.5$, respectively; hence it increases by 15.00% when K augments from 0 to 0.2 and it amplifies by 30.88% when K changes from 0 to 0.5. Whereas for GO-w nanofluids the values of $C_f \mathrm{Re}_x^{1/2}$ are 1.54380703, 1.80674982 and 2.07435846 when $K = 0$, $K = 0.2$ and $K = 0.5$, respectively and hence it uplifts by 17.03% when K grows from 0 to 0.2 and augments by 34.37% when K rises from 0 to 0.5.
- The Gr-w nanofluid delays the boundary layer separation more in comparison with GO-w nanofluid, i.e., less amount of wall mass suction needed for boundary layer flow of Gr-w nanofluid.
- The rise of permeability parameter K defers the boundary layer separation, whereas the higher nanoparticle volume fraction parameter ϕ calls it earlier.
- The surface-drag uplifts with K and S, whereas it declines with ϕ when S is approximately below 2.5 and later it boosts with ϕ. Also, surface-drag is comparatively higher for Gr-w nanofluid than GO-w nanofluid.
- The surface cooling rate coefficient $Nu_x \mathrm{Re}_x^{-1/2}$ upsurges with K and S, but it declines with ϕ and also $Nu_x \mathrm{Re}_x^{-1/2}$ is higher for Gr-w nanofluid than GO-w nanofluid.
- The velocity $f'(\eta)$ elevates with K and S, whereas it drops with ϕ. Importantly, Gr-w nanofluid have higher velocity than GO-w nanofluid.
- The temperature $\theta(\eta)$ boosts with ϕ and it decays with K, S and Pr. In addition, it is worthnoting that temperature in GO-w nanofluid is higher than Gr-w nanofluid.
- After the stability analysis, it is established that upper solution branches are physically stable and lower solution branches are unstable.

Table 3
Smallest eigenvalue, γ_1^* for few values of S with $\phi = 0.05$, $K = 0.2$ and Pr $= 6.2$.

S	Gr-W nanofluid		GO-W nanofluid	
	Upper branch	Lower branch	Upper branch	Lower branch
2.6	1.232153	−1.205098	1.194471	−1.167595
2.5	1.067290	−1.043682	1.028100	−1.004976
2.4	0.884192	−0.864815	0.840849	−0.822379
2.3	0.663318	−0.650349	0.609495	−0.598055
2.2	0.332931	−0.329005	0.219650	−0.217865
2.19	-	-	0.129316	−0.128704
2.186	-	-	0.064773	−0.064666
2.1847	-	-	0.011455	−0.011386
2.17	0.121340	−0.120789	-	-
2.166	0.045397	−0.045363	-	-
2.1654	0.013052	−0.013077	-	-

Funding information

The works of A.K. Verma[09/013(0724)/2017-EMR-I] and S. Rajput [09/013(0843)/2018-EMR-I] are funded by CSIR, India. K. Bhattacharyya also acknowledges “Faculty Incentive Grant” (No. R/Dev/D/IoE/Incentive/2022-23/47686) of Banaras Hindu University.

Declaration of Competing Interest

The authors declare that they have no known competing financial interests or personal relationships that could have appeared to influence the work reported in this paper.

Data Availability

No data was used for the research described in the article.

Acknowledgments

The authors are grateful to the reviewers for their precious comments and suggestions.

References

[1] E.G. Fisher, Extrusion of Plastics, Wiley, New York, 1976.
[2] L.J. Crane, Flow past a stretching plate, Z. Angew. Math. Phys. 21 (1970) 645–647.
[3] L.E. Erickson, L.T. Fan, V.G. Fox, Heat and mass transfer on a moving continuous flat plate with suction or injection, Ind. Eng. Che. Fund. 5 (1966) 19–25.
[4] V.G. Fox, L.E. Erickson, L.T. Fan, Methods for solving the boundary layer equations for moving continuous flat surfaces with suction and injection, AIChE J 14 (1968) 726–736.
[5] P.S. Gupta, A.S. Gupta, Heat and mass transfer on a stretching sheet with suction and blowing, Can. J. Chem. Eng. 55 (1977) 744–746.
[6] M.E. Ali, On thermal boundary layer on a power-law stretched surface with suction or injection, Int. J. Heat Fluid Flow. 16 (1995) 280–290.
[7] E. Magyari, B. Keller, Heat and mass transfer in the boundary layers on an exponentially stretching continuous surface, J. Phys. D: Appl. Phys. 32 (1999) 577.
[8] E.M.A. Elbashbeshy, Heat transfer over an exponentially stretching continuous surface with suction, Arch. Mech. 53 (2001) 643–651.
[9] M.K. Partha, P.V.S.N. Murthy, G.P. Rajasekhar, Effect of viscous dissipation on the mixed convection heat transfer from an exponentially stretching surface, Heat Mass Transf 41 (2005) 360–366.
[10] C.Y. Wang, Liquid film on an unsteady stretching surface, Q. Appl. Math. 48 (1990) 601–610.
[11] M. Miklavčič, C.Y. Wang, Viscous flow due a shrinking sheet, Q. Appl. Math. 64 (2006) 283–290.
[12] C.Y. Wang, Stagnation flow towards a shrinking sheet, Int. J. Nonlinear Mech. 43 (2008) 377–382.
[13] T. Fang, Boundary layer flow over a shrinking sheet with power-law velocity, Int. J. Heat Mass Transf. 5 (2008) 5838–5843.
[14] K. Bhattacharyya, Effects of heat source/sink on MHD flow and heat transfer over a shrinking sheet with mass suction, Chem. Eng. Res. Bull. 15 (2011) 12–17.
[15] T. Hayat, M. Hussain, A.A. Hendi, S. Nadeem, MHD stagnation point flow towards a heated shrinking surface subjected to heat generation/absorption, Appl. Math. Mech. 33 (2012) 631–648.
[16] K. Bhattacharyya, Boundary layer flow and heat transfer over an exponentially shrinking sheet, Chin. Phys. Lett. 28 (2011), 074701.
[17] K. Bhattacharyya, I. Pop, MHD boundary layer flow due to an exponentially shrinking sheet, Magnetohydrodynamics 47 (2011) 337–344.
[18] K. Bhattacharyya, K. Vajravelu, Stagnation-point flow and heat transfer over an exponentially shrinking sheet, Comm. Nonlinear Sci. Numerical Simul. 17 (2012) 2728–2734.
[19] D.S. Chauhan, R. Agarwal, MHD flow through porous medium adjacent to a stretching sheet: numerical and approximate solution, Eur. Phys. J. Plus. 126 (2011) 47.
[20] P. Vyas, N. Srivastava, Radiative MHD flow over a non-isothermal stretching sheet in a porous medium, Appl. Math. Scis. 4 (2010) 2475–2484.
[21] H. Rosali, A. Ishak, I. Pop, Stagnation point flow and heat transfer over a stretching/shrinking sheet in a porous medium, Int. Comm. Heat Mass Transf. 38 (2011) 1029–1032.
[22] P. Vyas, N. Srivastava, Radiative boundary layer flow in porous medium due to exponentially shrinking permeable sheet, Therm 2012 (2012) 1–9.
[23] S. Jain, R. Choudhary, Effects of MHD boundary layer flow in porous medium due to exponentially shrinking sheet with slip, Proc. Eng. 127 (2015) 1203–1210.
[24] I.L. Animasaun, Effects of thermophoresis, variable viscosity and thermal conductivity on free convective heat and mass transfer of non-Darcian MHD dissipative Casson fluid flow with suction and n-th order of chemical reaction, J. Nag. Math. Soci. 34 (2015) 11–31.
[25] S.S. Motsa, I.L. Animasaun, A new numerical investigation of some thermos-physical properties on unsteady MHD non-Darcian flow past an impulsively started vertical surface, Ther. Sci. 19 (2015) S249–S258.
[26] S.K. Das, S.U.S. Choi, W. Yu, T. Pradeep, Nanofluids: Science and Technology, Wiley, New York, 2007.
[27] S.U.S. Choi, Enhancing thermal conductivity of fluids with nanoparticles, in: D. A. Singer, H.P. Wang (Eds.), Developments and Applications of Non-Newtonian Flows, Amer. Soci. of Mech. Eng, New York, 1995, pp. 99–105. FED-231/MD-66.
[28] J.A. Eastman, S.U.S. Choi, S. Li, W. Yu, L.J. Thompson, Anomalously increased effective thermal conductivities of ethylene glycol based nanofluids containing copper nanoparticles, Appl. Phys. Lett. 78 (2001) 718.
[29] H.E. Patel, S.K. Das, T. Sundararajan, Thermal conductivities of naked and monolayer protected metal nanoparticle based nanofluids: manifestation of anomalous enhancement and chemical effects, Appl. Phys. Lett. 83 (2003) 2931.
[30] S.U.S. Choi, Z.G. Zhang, W. Yu, F.E. Lockwood, E.A. Grulke, Anomalous thermal conductivity enhancement in nano-tube suspension, Appl. Phys. Lett. 79 (2001) 2252.
[31] T.K. Hong, H.S. Yang, C.J. Choi, Study of the enhanced thermal conductivity of Fe nanofluids, J. Appl. Phys. 97 (2005), 064311.
[32] K.V. Wong, O.D. Leon, Applications of nanofluids: current and future, Adv. Mech. Eng. 2 (2010), 519659.
[33] J. Buongiorno, Convective transport in nanofluids, J. Heat Transf. 128 (2006) 240–250.
[34] R.K. Tiwari, M.K. Das, Heat transfer augmentation in a two-sided lid-driven differentially heated square cavity utilizing nanofluids, Int. J. Heat Mass Transf. 50 (2007) 2002–2018.
[35] W.A. Khan, I. Pop, Boundary-layer flow of a nanofluid past a stretching sheet, Int. J. Heat Mass Transf. 53 (2010) 2477–2483.
[36] N. Ishak, A. Hussanan, M.K.A. Mohamed, N. Rosli, M.Z. Salleh, Heat and mass transfer flow of a viscoelastic nanofluid over a stretching/shrinking sheet with slip condition, AIP Conf. Proc. 2059 (2019), 020011.
[37] S. Dero, A.M. Rohni, A. Saaban, Effects of the viscous dissipation and chemical reaction on Casson nanofluid flow over the permeable stretching/shrinking sheet, Heat Transf 49 (2020) 1736–1755.
[38] I. Rashid, M. Sagheer, S. Hussain, Entropy formation analysis of MHD boundary layer flow of nanofluid over a porous shrinking wall, Phys. A: Stat. Mech. Applic. 536 (2019), 122608.
[39] Y.D. Reddy, V.S. Rao, M.A. Kumar, Effect of heat generation/absorption on MHD copper-water nanofluid flow over a nonlinear stretching/shrinking sheet, AIP Conf. Proc. 2246 (2020), 020017.
[40] S.K. Rawat, M. Kumar, Cattaneo-Christov heat flux model in flow of copper water nanofluid through a stretching/shrinking sheet on stagnation point in presence of heat generation/absorption and activation energy, Int. J. App. Comp. Math. 6 (2020) 112.
[41] D. Yang, M. Yasir, A. Hamid, Thermal transport analysis in stagnation-point flow of Casson nanofluid over a shrinking surface with viscous dissipation, Waves Random Complex Media (2021), https://doi.org/10.1080/17455030.2021.1972183.
[42] M.N. Khan, S. Nadeem, MHD stagnation point flow of a Maxwell nanofluid over a shrinking sheet (multiple solution), Heat Transf 50 (2021) 4729–4743.
[43] S.A. Jumana, M.G. Murtaza, M. Ferdows, O.D. Makinde, K. Zaimi, Dual solutions analysis of melting phenomenon with mixed convection in a nanofluid flow and heat transfer past a permeable stretching/shrinking sheet, J. Nanofluid. 9 (2020) 313–320.
[44] K.S. Tshivhi, O.D. Makinde, Magneto-nanofluid coolants past heated shrinking/stretching surfaces: dual solutions and stability analysis, Result. Eng. 10 (2021), 100229.
[45] S. Naramgari, C. Sulochana, Dual solutions of radiative MHD nanofluid flow over an exponentially stretching sheet with heat generation/absorption, Appl. Nanosci. 6 (2016) 131–139.
[46] Y.X. Li, M.H. Alshbool, Y.P. Lv, I. Khan, M.R. Khan, A. Issakhov, Heat and mass transfer in MHD Williamson nanofluid flow over an exponentially porous stretching surface, Case Stud. Ther. Eng. 26 (2021), 100975.
[47] A. Ali, K. Shehzadi, M. Sulaiman, S. Asghar, Heat and mass transfer analysis of 3D Maxwell nanofluid over exponentially stretching surface, Phys. Scr. 94 (2019), 065206.
[48] N.A. Zainal, R. Nazar, K. Naganthran, I. Pop, Heat generation/absorption effect on MHD flow of hybrid nanofluid over bidirectional exponential stretching/shrinking sheet, Chi, J. Phys. 69 (2019) 118–133.
[49] N.A. Zainal, R. Nazar, K. Naganthran, I. Pop, Viscous dissipation and MHD hybrid nanofluid flow towards an exponentially stretching/shrinking surface, Neural Comp. Appl. 33 (2021) 11285–11295.
[50] S. Ghosh, S. Mukhopadhyay, Flow and heat transfer of nanofluid over an exponentially shrinking porous sheet with heat and mass fluxes, Prop. Pow. Res. 7 (2018) 268–275.
[51] S. Ghosh, S. Mukhopadhyay, Stability analysis for model-based study of nanofluid flow over an exponentially shrinking permeable sheet in presence of slip, Neural Comput. Appl. 32 (2020) 7201–7211.
[52] Q.H. Shi, B.S. Ahmed, S. Ahmad, S.U. Khan, K. Sultan, M.N. Bashir, M.I. Khan, N. A. Shah, J.D. Chung, Dual solution framework for mixed convection flow of Maxwell nanofluid instigated by exponentially shrinking surface with thermal radiation, Sci. Rep. 11 (2021) 15944.
[53] I. Waini, A. Ishak, I. Pop, Hybrid nanofluid flow induced by an exponentially shrinking sheet, Chin. J. Phys. 68 (2020) 468–482.
[54] M. Sheikholeslami, Z. Ebrahimpour, Thermal improvement of linear Fresnel solar system utilizing Al_2O_3-water nanofluid and multi-way twisted tape, Int. J. Ther. Sci. 176 (2022), 107505.
[55] M. Sheikholeslami, Z. Said, M. Jafaryar, Hydrothermal analysis for a parabolic solar unit with wavy absorber pipe and nanofluid, Ren. Ener. 188 (2022) 922–932.
[56] M. Sheikholeslami, M. Jafaryar, M.B. Gerdroodbary, A.H. Alavi, Influence of novel turbulator on efficiency of solar collector system, Env. Tech. Inn. 26 (2022), 102383.
[57] M. Sheikholeslami, S.A. Farshad, Nanoparticles transportation with turbulent regime through a solar collector with helical tapes, Adv. Powd. Tech. 33 (2022), 103510.
[58] M. Sheikholeslami, Numerical investigation of solar system equipped with innovative turbulator and hybrid nanofluid, Solar Energy, Mat. Solar Cells. 243 (2022), 111786.
[59] M. Sheikholeslami, Analyzing melting process of paraffin through the heat storage with honeycomb configuration utilizing nanoparticles, J. Ener. Stor. 52 (2022), 104954.
[60] S. Saleem, I.L. Animasaun, Se-Jin Yook, Q.M. Al-Mdallal, N.A. Shah, M. Faisal, Insight into the motion of water conveying three kinds of nanoparticles shapes on a horizontal surface: significance of thermo-migration and Brownian motion, Surf. Int. 30 (2022), 101854.
[61] W. Cao, I.L. Animasaun, S.-.J. Yook, V.A. Oladipupo, X. Ji, Simulation of the dynamics of colloidal mixture of water with various nanoparticles at different levels of partial slip: ternary-hybrid nanofluid, Int. Comm. Heat Mass Transf. 135 (2022), 106069.
[62] I.L. Animasaun, S.-.J. Yook, T. Muhammad, A. Mathew, Dynamics of ternary-hybrid nanofluid subject to magnetic flux density and heat source or sink on a convectively heated surface, Surf. Interf. 28 (2022), 101654.
[63] A. Kasaeian, R.D. Azarian, O. Mahian, L. Kolsi, A.J. Chamkha, S. Wongwises, I. Pop, Nanofluid flow and heat transfer in porous media: a review of the latest developments, Int. J. Heat Mass Transf. 107 (2017) 778–791.

[64] T. Hayat, M. Imtiaz, A. Alsaedi, R. Mansoor, MHD flow of nanofluids over an exponential stretching sheet in a porous medium with convective boundary conditions, Chin. Phys. B. 23 (2014), 054701.
[65] M.K. Nayak, S. Shaw, O.D. Makinde, Chemically reacting and radiating nanofluid flow past an exponentially stretching sheet in a porous medium, Ind. J. Pure Appl. Phys. 56 (2018) 773–786.
[66] R.P. Sharma, A.K. Jha, P.K. Gaur, S.R. Mishra, Nanofluid motion past shrinking sheet in porous media under the impact of radiation and heat source/sink, Int. J. Appl. Mech. Eng. 24 (2019) 183–199.
[67] R. Ul Haq, A. Raza, E.A. Algehyne I. Tlili, Dual nature study of convective heat transfer of nanofluid flow over a shrinking surface in a porous medium, Int. Comm. Heat Mass Transf. 114 (2020), 104583.
[68] H.M. Shawky, N.T.M. Eldabe, K.A. Kamel, E.A. Abd-Aziz, MHD flow with heat and mass transfer of Williamson nanofluid over stretching sheet through porous medium, Micro. Technol. 25 (2019) 1155–1169.
[69] F.B. Tadesse, O.D. Makinde, L.G. Enyadene, Hydromagnetic stagnation point flow of a magnetite ferrofluid past a convectively heated permeable stretching/shrinking sheet in a Darcy-Forchheimer porous medium, Sādhanā 46 (2021) 1–17.
[70] F.B. Tadesse, O.D. Makinde, L.G. Enyadene, Mixed convection of a radiating magnetic nanofluid past a heated permeable stretching/shrinking sheet in a porous medium, Math. Prob. Eng. 2021 (2021), 6696748.
[71] D. Dey, O.D. Makinde, R. Borah, Analysis of dual solutions in MHD fluid flow with heat and mass transfer past an exponentially shrinking/stretching surface in a porous medium, Int. J. Appl. Comp. Math. 8 (2022) 66.
[72] C. Chung, Y.K. Kim, D. Shin, S.R. Ryoo, B.H. Hong, D.H. Min, Biomedical applications of graphene and graphene oxide, Acc. Chem. Res. 46 (2013) 2211–2224.
[73] A. Rehman, Z. Salleh, T. Gul, Z. Zaheer, The impact of viscous dissipation on the thin film unsteady flow of GO-EG/GO-W nanofluids, Mathematics 7 (2019) 653.
[74] A.H.C. Netro, F. Guinea, N.M.R. Peres, K.S. Novoselov, A.K. Geim, The electronic properties of grapheme, Rev. Mod. Phys. 81 (2009) 109.
[75] S.M. Upadhya, C.S.K. Raju, S. Saleem, A.A. Alderremy, Mahesha, Modified Fourier heat flux on MHD flow over stretched cylinder filled with dust, graphene and silver nanoparticles, Result Phys. 9 (2018) 1377–1385.
[76] R. Sharma, C.S. Raju, I.L. Animasaun, H.B. Santhosh, M.K. Mishra, Insight into the significance of Joule dissipation, thermal jump and partial slip dynamics of unsteady ethylene glycol conveying graphene nanoparticles through porous medium, Nonlinear Eng 10 (2021) 16–27.
[77] S.M. Hussain, R. Sharma, M.R. Mishra, S.S. Alrashidy, Hydromagnetic dissipative and radiative graphene Maxwell nanofluid flow past a stretched sheet-numerical and statistical analysis, Mathematics 8 (2020) 1929.
[78] E.H. Aly, Dual exact solutions of graphene–water nanofluid flow over stretching/shrinking sheet with suction/injection and heat source/sink: critical values and regions with stability, Powder Tech 342 (2019) 528–544.
[79] U. Rashid, D. Baleanu, H. Liang, M. Abbas, A. Iqbal, J. Ul Rahman, Marangoni boundary layer flow and heat transfer of graphene-water nanofluid with particle shape effects, Processes 8 (2020) 1120.
[80] N. Sandeep, A. Malvandi, Enhanced heat transfer in liquid thin film flow of non-Newtonian nanofluids embedded with graphene nanoparticles, Adv. Powder Tech. 27 (2016) 2448–2456.
[81] T. Gul, H. Anwar, M.A. Khan, I. Khan, P. Kumam, Integer and non-integer order study of the GO-W/GO-EG nanofluids flow by means of Marangoni convection, Symmetry (Basel) 11 (2019) 640.
[82] A. Hamid, A.Hafeez Hashim, M. Khan, A.S. Alshomrani, M. Alghamdi, Heat transport features of magnetic water–graphene oxide nanofluid flow with thermal radiation: stability test, Eur. J. Mech.-B Fluids. 76 (2019) 434–441.
[83] A. Javanmard, M.H. Taheri, M. Abbasi, S.M. Ebrahimi, Heat transfer analysis of hydromagnetic water-graphene oxide nanofluid flow in the channel with asymmetric forced convection on walls, Che. Eng. Res. Des. 136 (2018) 816–824.
[84] H.F. Oztop, E. Abu-Nada, Numerical study of natural convection in partially heated rectangular enclosures filled with nanofluids, Int. J. Heat Fluid Flow 29 (2008) 1326–1336.
[85] K. Bhattacharyya, G.C. Layek, G.S. Seth, Soret and Dufour effects on convective heat and mass transfer in stagnation-point flow towards a shrinking surface, Phys. Scr. 89 (2014), 095203.
[86] S. Rajput, A.K. Pandey, K. Bhattacharyya, I. Pop, Effect of convective boundary condition on unsteady flow of CNT-H_2O nanofluid towards a stagnation-point on a shrinking/expanding flat sheet, Proc. Inst. Mech. Eng. E: J. Process Mech. Eng. 236 (2022) 1023–1033.
[87] S. Rajput, K. Bhattacharyya, A.K. Verma, M.S. Mandal, A.J. Chamkha, D. Yadav, Unsteady stagnation-point flow of CNTs suspended nanofluid on a shrinking/expanding sheet with partial slip: multiple solutions and stability analysis, Waves Random Complex Media (2022), https://doi.org/10.1080/17455030.2022.2063986.
[88] J.H. Merkin, On dual solutions occurring in mixed convection in a porous medium, J. Eng. Math. 20 (1985) 171–179.
[89] P.D. Weidman, D.G. Kubitschek, A.M.J. Davis, The effect of transpiration on self-similar boundary layer flow over moving surfaces, Int. J. Eng. Sci. 44 (2006) 730–737.
[90] S.D. Harris, D.B. Ingham, I. Pop, Mixed convection boundary layer flow near the stagnation point on a vertical surface in a porous medium: Brinkman model with slip, Trans. Porous Media. 77 (2009) 267–285.